The Effect of Solvation Shell Structure and Composition on Ion Pair Formation: The Case Study of LiTDI in Organic Carbonates

*Jeramie C. Rushing, Fedra M Leonik and Daniel G. Kuroda**

Department of Chemistry, Louisiana State University, Baton Rouge, Louisiana 70803, United States

*Address correspondence to dkuroda@lsu.edu

ABSTRACT

Organic carbonates are integral to the desirable properties of commercial lithium ion batteries due to their high dielectric constants. However, the high viscosity of organic carbonates requires the use of mixtures containing a cyclic and a linear carbonate. In binary mixtures, the linear and cyclic organic carbonates compete to solvate the lithium salt. While the preferential solvation has been extensively studied, the effect of the mixed solvation on the ionic speciation of the lithium ion is a topic which has not been studied in detail. In this study, infrared spectroscopies and ab-initio chemical computations are utilized to study the change in the solvation structure and dynamics as a function of solvent composition for the model system: lithium 4,5-dicyano-2-(trifluoromethyl)imidazole (LiTDI). The TDI- nitrile bands are used to probe the changes in the ion speciation as well as in the molecular environment, since nitriles are known to be good and sensitive IR spectroscopic reporters of the environment. Our experimental finding shows that the anion forms contact ion pairs, but the amount of contact ion pairs is strongly dependent on the type of carbonate. In particular, TDI- has strong propensity of forming contact ion pairs in linear carbonates, while in cyclic carbonates is primarily not directly interacting with Li+. The dynamics of the environment support our speciation of the anion in both solvents. In addition, the concentration of contact ion pairs shows a monotonic and non-linear increase with the concentration of linear carbonate in the mixture. Ab-initio computations reveal that the non-linear behavior is related to the energetics of ion pair formation, which appears to be much more favorable when the lithium solvation shell does not contain cyclic carbonates. Overall, our results show that the concentration of linear carbonates in a mixture of organic carbonates directly influences the speciation of the lithium ion.

INTRODUCTION

Lithium ion batteries have become the standard technology in energy storage over the last 25 years. While this battery technology is particularly ubiquitous to the energy demands of portable electronics,[1] lithium ion batteries have also found its use in rechargeable power tools and electric vehicles.[1-2] Looking into the future, substantial effort is expected for implementing lithium ion energy storage technologies in power grids.[3-4] Thus, the rapid global adoption of lithium ion batteries has led to considerable interest in researching new materials and technologies to improve battery efficiency and lower costs. However, there is a knowledge gap of the batteries currently on the market, arising from the lack of molecular level understanding of the electrochemical components of the device.[5] More precisely, identifying the molecular-level interactions in the electrode, electrolytes, and their interphases has remained a grand challenge in science.[5]

Common electrolyte solvents for lithium ion batteries are comprised of a mixture of one linear carbonate, such as dimethyl carbonate (DMC) or ethyl methyl carbonate (EMC), and one cyclic carbonate, such as ethylene carbonate (EC), propylene carbonate (PC), or butylene carbonate (BC).[5] Cyclic carbonates are chosen for their large dielectric constants, while linear carbonates are utilized for their low viscosity.[5-6] Thereby, linear and cyclic carbonates are both critical to the design of a functional electrolyte. However, in the mixture of carbonates, each solvent competes to solvate the lithium ion (Li+) and the anion. As such, the presence of two different solvents has significant consequences on the solvation structure of the cation and anion.

It has been shown for commercially available electrolytes, composed of lithium hexafluorophosphate ($LiPF_6$) in organic carbonates, that the structure of the Li+ solvation shell is determined by the structure of the nearby solvent molecules.[7-8] For example, it has been found that

linear organic carbonates form a more compact solvation shell than their cyclic analogues. In the latter case, the solvation shell is more extended due to the interaction between molecules in the first and second solvation shell.[9] In addition, it is apparent that the solvation structure of Li+ also dictates its speciation in solution.[8,10-12] Moreover, the electrolyte properties, such as conductivity, are drastically different depending on which solvent solvates Li+ and its counter-ion.[13-15] While there have been previous investigations of the effect of the solvation shell in the solvation of Li+,[8,16-17] questions remain about the effect of mixed solvation on solvation structure of organic carbonate electrolytes. In particular, there are contradictory findings regarding the mixtures of organic carbonates. For example, studies have concluded that linear carbonates preferentially solvate Li+,[8] while others favor the cyclic carbonate in this role.[18-19] Further complicating matters, other studies have concluded that preferential solvation is concentration dependent in mixtures of organic carbonates,[20] but not in mixtures of a cyclic organic carbonate and water.[21] It is also interesting that the preferential solvation is structurally dependent,[22] but the observed order (i.e., ethylene carbonate > dimethyl carbonate > vinylene carbonate) does not necessary follow the dielectric constant of the solvent. In addition, it has been observed that propylene carbonate presents dipolar ordering in solution,[23] indicating that solvent-solvent interactions could play a role in the preferential solvation. Moreover, it has been recently demonstrated that solvent-solvent interaction are key in defining the lithium ion solvation shell structure and dynamics formed in pure cyclic carbonates.[7,24-25] These conflicting results clearly illustrate the merit for studying lithium salts in mixtures of organic carbonates.

While the preferential solvation by organic carbonates is a topic extensively studied,[25-28] the role of the mixed solvation shell in the speciation of Li+ is a topic vastly unexplored. So far, most studies have focused on either lithium hexafluorophosphate ($LiPF_6$) or lithium

bis(trifluoromethanesulfonyl)imide (LiTFSI),[8,20,29-30] but the lack of simple vibrational modes in PF_6- and TFSI- has complicated their analysis and interpretation.[8,17,31-32] Thus, this study focuses on the effect of carbonate structure and composition on the speciation of lithium 4,5-dicyano-2-(trifluoromethyl)imidazole salt (LiTDI, Scheme 1).

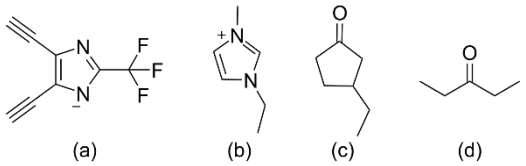

Scheme 1. Structures for (a) 4,5-dicyano-2-(trifluoromethyl)imidazole (TDI-), (b) 1-ethyl-3-methylimidazole (EMIM), (c) 1,2-butylene carbonate (BC) and (d) dimethyl carbonate (DMC).

LiTDI has been subject to many recent studies due to its potential as an alternative to $LiPF_6$ in electrolytes. To this end, the properties of LiTDI in various electrolytes have been explored. In particular, the physicochemical and electrochemical properties of LiTDI in solvents such as acetonitrile,[33] propylene carbonate,[34-35] methyl and ethyl ethers of poly(ethylene glycol),[36] poly(ethylene oxide),[37] mixed carbonate solvents, [38] and ionic liquids[39] have been studied. Other studies on LiTDI have concentrated on the interaction and coordination of Li+ and the anion in solution,[40] and solvates.[41] Overall, these studies have shown that nitrile (-CN) groups are sensitive infrared probes to the speciation of TDI-.[42-43] In particular, it has been derived that TDI- forms ion pairs with Li+ at low concentrations in mixed solvents, in spite of the strong delocalization of the charge in the anion.[38] While the effect of a mixed solvent on the speciation of LiTDI has been studied from the conductivity and transport number perspective,[38,44] the molecular origins behind the speciation of LiTDI in the different carbonate solutions are still unknown.

This study focuses on the speciation of LiTDI in pure linear and cyclic carbonates as well as their mixtures using linear infrared (FTIR) and time-resolved infrared spectroscopies. Two dimensional IR (2DIR) spectroscopy is used because it can determine the dynamics processes,

such as solvation shell reorganization and ion pair formation, on picosecond timescales, which is well beyond the capabilities of other commonly used characterization spectroscopies, such as NMR.[45] Furthermore, 2DIR spectroscopy also features high frequency resolution and a second dimension, which provide one not only with the opportunity of resolving peaks not seen in linear spectra,[46-47] but also with the possibility of determining vibrational coupling among vibrational transitions.[45,48-50] This last feature is an essential characteristic for correctly assigning vibrational peaks and their assignment to different species.[45,50-51] These two characteristics grant 2DIR spectroscopy with unique insights into the structure and dynamics of systems at a molecular level. In particular, 2DIR spectroscopy has been successfully used to study the ion-ion and ion-solvent interactions in a variety of systems.[9,52-58] Thus, the use of FTIR and 2DIR allows us to study the structure and dynamics of LiTDI in organic carbonates, as well as to obtain the speciation of the ion. To this end, our study of LiTDI is focused on each pure solvent (DMC and BC) and on their mixtures. The LiTDI salt is employed due to its well-documented sensitivity to solvent environment[59-62] and spectrally-isolated infrared bands.[63] Our experimental results provide a molecular picture of the anion solvation structure and dynamics, which are complemented with computational calculations to validate the modeling of our findings.

METHODS

Sample preparation. Lithium 4,5-dicyano-2-(trifluoromethyl)imidazole (LiTDI, Alfa Aesar, 95% pure) was dried at 140° C for 15 hours under vacuum before use and stored in a N_2-filled glovebox. 1-ethyl-3-methylimidazolium 4,5-dicyano-2-(trifluoromethyl)imidazole ((EMIM)TDI) was synthesized in 95% purity (by NMR) according to Ref. [39]. Dimethyl carbonate (DMC, 99+% Acros Organics), ethyl methyl carbonate (EMC, >98% TCI), propylene carbonate (PC, 99.5% Acros Organics), and 1,2-butylene carbonate (BC, 98% TCI) were all dried under activated 4A

molecular sieves prior to use to remove water. All components were stored in a N_2-filled glovebox to minimize exposure to moisture. In addition, all solutions and samples were prepared inside the glovebox. All samples tested <200 ppm of water after preparation.

Sample cells were prepared in a N_2-filled glovebox by sandwiching the LiTDI solution between two CaF_2 windows with a 6 μm spacer. The same preparation was used for both FTIR and 2DIR sample cells for experiments in the nitrile IR stretch region (2100-2300 cm^{-1}). All 2DIR experiments were conducted at the same concentration (X_{Li} = 0.05) because of the poor solubility of the salt in linear carbonates (i.e., DMC and EMC). In this case, X_{Li} is defined as the moles of Li+ over the total moles of Li+ and solvent. Also, FTIR sample cells used in the carbonyl IR stretch region (1700-1900 cm^{-1}) were prepared by sandwiching the sample between two CaF_2 windows without a spacer to minimize the high absorbance for the carbonyl band of the organic carbonate.[7] The approximate path length of this latter cell is ~1-2 μm.

FTIR Spectroscopy. FTIR spectra were taken on a Bruker Tensor 27 spectrometer with a 0.5 cm^{-1} resolution. Forty scans were averaged for each spectrum.

2D IR Spectroscopy. The setup used for 2DIR experiments has been previously detailed in the literature, so only a short description is provided here.[45,64] The input IR pulses were generated with a Spectra Physics Spitfire Ace Ti:sapphire amplifier at a repetition rate of 5 kHz, in combination with an OPA-800C and difference frequency generation crystal. These input IR pulses were then split into 3 replicas and later focused on the sample using the well-known boxcars geometry.[65] The photon echo signal was measured in the $\mathbf{-k_1+k_2+k_3}$ phase-matching direction. A heterodyned detection was performed using a forth pulse (local oscillator). The heterodyned signal was measured in a 64 element MCT array detector after dispersing the heterodyned signal in a spectrometer. The photon echo signal was measured as a function of three critical time intervals:

the coherence time τ (interval between pulses 1 and 2), the waiting time T_W (interval between pulses 2 and 3), and the coherence time t (interval between pulse 3 and the detected signal). These time intervals were set via computer-controlled translation stages. Here, 2D IR data were collected by scanning τ time from -4 ps to +4 ps in increments of 5 fs for each waiting time in order to collect both the rephasing and non-rephasing data by switching the time ordering.[45] Signals were collected for waiting times from 0 to 5 ps in steps of 0.5 ps. Note that the data collection in waiting was confined to a maximum of 5 ps due to the presence of heating effects (see supporting information). In all the measurements, the local oscillator always preceded the photon echo signal by ~0.5 ps. The time domain signal, collected as function of (τ,T, λ_t) via a monochromator-array detection, is transformed into the 2DIR spectra (ω_τ, T, ω_t) by means of Fourier transforms. A detailed explanation of the Fourier analysis has been described elsewhere.[48]

DFT calculations. Density functional theory (DFT) frequency calculations were conducted in Gaussian 09 software.[66] Geometry optimizations and frequency calculations were conducted using DFT with B3YLP functional and the 6-311++G** basis set. This functional and basis set has been successfully used to investigate the energetics and IR frequencies of lithium ion solvation structures and its ion pairing.[8,17,34,67-68] Initial molecules were built in the Avogadro software and the structures were first minimized using a classical force field (MMFF94). All geometries were optimized in Gaussian 09. Geometry optimizations and frequency calculations were performed in vacuum since the addition of a dielectric continuum has been shown to not change the trends in the Li+ solvation.[69] After minimization, molecules did not present imaginary frequencies confirming each structure as a minimum on the potential energy surface. The energy of ion pair formation as function of solvation shell structure and composition was computed using the same procedure as Ref. [70]. The natural bond orbital analysis (NBO) was used to calculate the atomic

partial charges.[71-73] NBO was performed at the same level of theory (B3LYP/6-311++G**) using the NBO software implemented in Gaussian 09 software.

RESULTS

The characterization of the solvation shell of Li+ was performed by measuring the IR spectra in the carbonyl stretch region (1700-1900 cm^{-1} region). FTIR spectra of different concentration solutions of LiTDI (X_{Li} = 0.01, 0.025, and 0.05) in DMC and BC are shown in Figure 1. The IR spectra display a high-intensity band located at 1755 cm^{-1} and at 1797 cm^{-1} for DMC and BC, respectively. A low frequency band, located at 1725 cm^{-1} for DMC and at 1765 cm^{-1} for BC, rises with increasing Li+ concentration in the solution. Due to its growth with increasing Li+ concentration, the low frequency band has been previously assigned to the carbonyl stretch of carbonate molecules coordinated to Li+.[5,8,42] Similarly, the high frequency band has been previously assigned to the free carbonyl stretch of the solvent.[5,8,42]

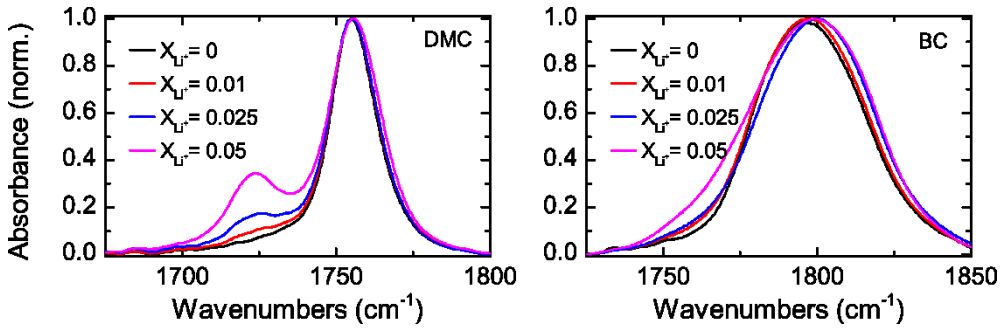

Figure 1. FTIR spectra for the carbonyl region of LiTDI as function of concentration: X_{Li} = 0.00 (black), 0.01 (red), 0.025 (blue), and 0.05 (pink) in DMC (left panel) and BC (right panel). XLi = 0.00 corresponds to the sample containing (EMIM)TDI with XEMIM=0.05 Both spectra are normalized with respect to the high frequency band.

The characterization of the TDI- solvation was performed by measuring the IR spectra in the CN stretch region (2150-2300 cm^{-1}). Figure 2 shows the IR spectra of LiTDI in DMC and BC as a function of Li+ concentration (X_{Li} = 0.00, 0.01, 0.025, and 0.05). Note that the sample with

X_{Li} = 0.00 corresponds to the sample containing (EMIM)TDI with X_{EMIM}=0.05. In both carbonate solutions, a low frequency band (2230 cm^{-1} for DMC, 2225 cm^{-1} for BC) and a high frequency band (2247 cm^{-1} for DMC, 2245 cm^{-1} for BC) are observed. The high frequency bands grow with increasing Li+ concentration in both samples, but it always remains significantly higher for DMC than BC solutions with equal X_{Li}. For comparison purposes, the FTIR spectra of (EMIM)TDI at X_{EMIM} = 0.05 in DMC and BC are also displayed in Figure 2. Interestingly, (EMIM)TDI shows only one peak at 2225 cm^{-1} in both solvents. Note that the small peak at 2250 cm^{-1} observed in the (EMIM)TDI in both solvents arises from either the residual Li+ or an impurity from its synthesis (see methods section). While the peak position of TDI- presents the same frequency position for (EMIM)TDI and LiTDI in BC, a shift of ~5 cm^{-1} is observed for the DMC solution. The difference between the CN stretch bands of TDI- in samples containing Li+ and EMIM+ is attributed to the different speciation of the TDI- in the two solvents.

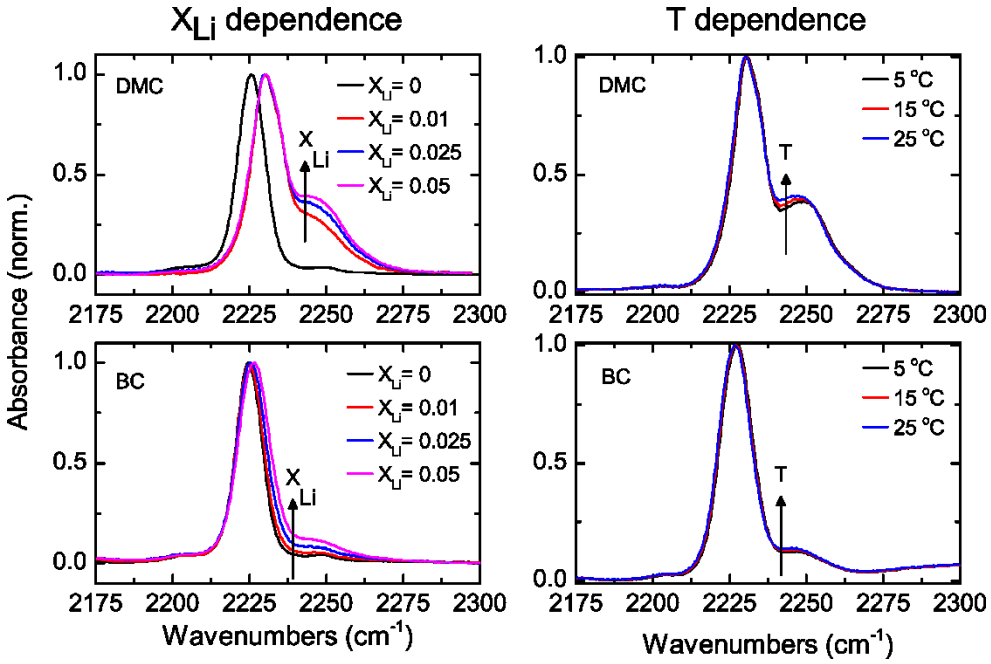

Figure 2. FTIR spectra for the nitrile region of LiTDI. Left panels concentration dependence of LiTDI for X_{Li} = 0.01, 0.025, and 0.05 in DMC (top) and BC (bottom) and (EMIM)TDI (X_{Li} = 0.00 and X_{EMIM} = 0.05) for comparison. Right panels temperature dependence of LiTDI (X_{Li} = 0.05) in

DMC (top) and BC (bottom) for 5 °C, 15 °C, and 25 °C. All spectra are normalized with respect to the low frequency band.

The assignment of the CN stretch peaks is further investigated by temperature-dependent FTIR. The IR spectra of the LiTDI samples with X_{Li}=0.05 as function of temperature is displayed in Figure 2. Both samples present two discernable changes with temperature: a small frequency shift and a change in the ratio of absorptions between the two frequency bands, in which the high frequency band grows with respect to the low frequency band with increasing temperature. These spectral changes with temperature are also in agreement with the difference spectra (see supporting information).

TDI- was further investigated by measuring the 2DIR spectra. The 2D IR spectra for LiTDI in DMC and BC are presented in Figure 3 for waiting times 0 ps, 2.5 ps, and 5 ps. As in the FTIR spectra, two sets of peaks are observed at ω_τ = 2230 cm^{-1} and ω_τ = 2247 cm^{-1} for DMC and at ω_τ = 2225 cm^{-1} and ω_τ = 2245 cm^{-1} for BC. In the 2DIR spectra, the red (positive) peaks located in the diagonal (ω_τ= ω_t = 2025 cm^{-1} for DMC, ω_τ= ω_t = 2030 cm^{-1} for BC) represent the transitions between ν=0 and ν=1 vibrational states, and blue (negative) peaks down shifted by ~25 cm^{-1} depict the transitions between ν=1 to ν=2 vibrational states.[45] The downshifts of the blue peaks with respect to the red peaks denotes the anharmonic nature of CN stretch potential of TDI- and is in agreement with other aromatic nitrile groups.[74] The 2DIR spectra also demonstrate that the intensity of the low frequency peak is always greater than that of the higher frequency peak in both solvents. Moreover, the high frequency peak has a larger intensity for DMC than BC. In fact, in the latter case, the high frequency peak is substantially weaker in the 2DIR spectra. The observed number of diagonal peaks and their intensities in the 2DIR have the expected direct correspondence with the linear IR spectra for the two samples.

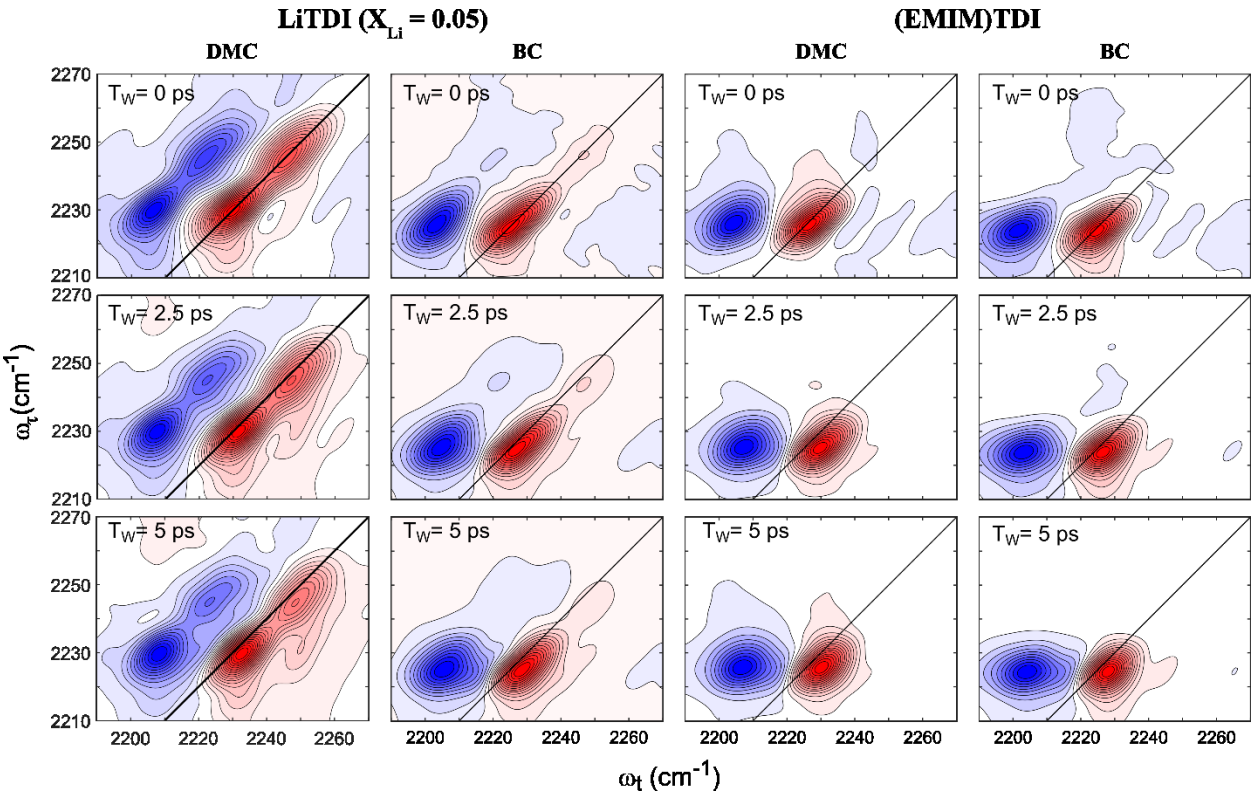

Figure 3. 2D IR spectra for the nitrile region of LiTDI (X_{Li} = 0.05) and (EMIM)TDI (X_{EMIM} = 0.05) in DMC and BC. The presented spectra corresponds to three waiting times: 0 ps, 2.5 ps, and 5 ps.

The 2DIR spectra do not display significant changes in the shape of the peaks with waiting time (T_W) besides the changes in intensity given by the vibrational population lifetime. In other words, the peaks initially elongated along the diagonal remain nearly unchanged as T_W progresses. A small cross peak is also present at T_W = 0 ps at $[\omega_\tau,\omega_t]$=[2230 cm^{-1}, 2250 cm^{-1}] for DMC, but it is not appreciable in the 2DIR of LiTDI in BC at the zero waiting time. However, the cross peak appears to grow with increasing T_W for both DMC and BC. Moreover, the cross peak growth in the BC sample is also corroborated by the waiting time evolution of the integrated sections of the 2DIR spectra (see supporting information). The presence of cross peaks is evidence of a vibrational coupling between the two CN stretch modes of TDI- (see next section).[45,50,75] For comparison, 2DIR spectroscopy was also performed on (EMIM)TDI in DMC and BC samples. In these later

samples, only one set of peaks was observed at ω_τ = 2225 cm^{-1} irrespective of the solvent. In addition, the peaks appear to become rounder with waiting time in both cases, contrasting with LiTDI samples where no apparent evolution is observed with T_W.

Finally, the FTIR spectroscopy of LiTDI (X_{Li} = 0.05) in DMC/BC, DMC/EMC, and BC/PC solvent mixtures were investigated (Figure 4). For mixtures, two bands located at 2225 cm^{-1} and 2250 cm^{-1} are observed with the low frequency band having a larger intensity in all samples at all compositions. While the mixtures of linear carbonates (DMC/EMC) and cyclic carbonates (BC/PC) do not appear to show substantial changes in the band areas with solvent composition, the linear and cyclic mixture (DMC/BC) shows that the low frequency band shifts its frequency position to higher values as the concentration of DMC increases in the solvent. In addition, there is a large change in the ratio of absorptions between the two CN stretch bands as the solvent composition changes from pure BC to pure DMC.

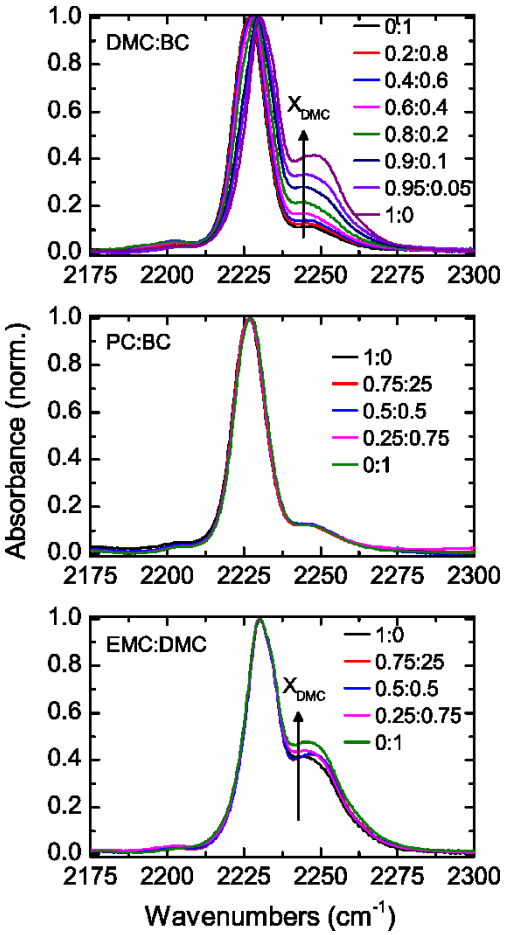

Figure 4. FTIR spectra for the nitrile region of LiTDI (X_{Li} = 0.05) as a function of solvent composition. The mixed solvent data is representative of [X:1-X] ratios as indicated in the figure for DMC:BC (top), PC:BC (middle) and EMC:DMC (bottom).

DISCUSSION

Pure carbonates

The speciation of TDI- is directly related to the overall solvation of Li+. Based on previous assignments of the bands in the 1700-1900 cm^{-1} region, the appearance of a low-frequency band in the C=O stretch region (Figure 1) shows that some carbonates are directly coordinated to Li+.[42] While the solvation of Li+ through the carbonyl bands is evident, the complex nature of the carbonyl band does not allow us to conclude whether Li+ is fully solvated by the solvent or is

forming contact ion pairs.[7,32] However, the results show that even in the case of Li+ and TDI forming contact ion pair, the majority of Li+ must be partially solvated by carbonates.

From the anion perspective, the nitrile stretch region provides a direct window to investigate the anion. The spectra of (EMIM)TDI in both solvents (Figure 2) presents only one band at 2225 cm^{-1}. Since the imidazolium cation has a delocalized charge, it is unlikely that EMIM+ will form contact ion pairs (CIP) with TDI- or affect its vibrational manifold.[39,76] Thus the band at 2225 cm^{-1} is assigned as the free anion band in pure BC and DMC. It is important to note that the free anion band is comprised of two transitions, the asymmetric and symmetric nitrile stretches.[34] The two combination modes of CN stretches are nearly-degenerate in the free species because the solvent lacks sufficiently large and directional interactions to break the symmetry of the molecule, but the non-degeneracy can explain the small asymmetry of the TDI- peak towards the high frequency side. The presence of Li+ in the TDI- solutions produces the growth of a second peak at ~2245 cm^{-1} in DMC and BC pure solvents. The appearance of the high frequency peak denotes the formation of contact ion pairs as previously demonstrated.[34,38] In the case of CIPs, the coordination of Li+ to TDI- breaks the symmetry of the molecule, which shifts the frequency of one of the CN modes to ~20 cm^{-1} higher than that observed for the free ion (i.e., (EMIM)TDI solution). While the same splitting and the growth of the high frequency band with Li+ concentration is observed for LiTDI in both carbonates, the intensity of the high frequency band is much greater in DMC than BC solution. While this result could be interpreted as a change in the oscillator strength of TDI- and the different ion pairs, DFT computations show that the oscillator strength is similar for TDI- as free ion, SSIP, and CIPs with different carbonates (see supporting information). Thus, the appearance of the high frequency band shows that the structure of the organic carbonate affects the formation of contact ion pairs, which is in agreement with previous

studies.[7,38] In particular, it shows that CIP species are more prevalent in linear carbonates, which differs with other anions such as hexafluorophosphate (PF6-) ions and bis(trifluoromethanesulfonyl)imide (TFSI) ions at the same concentrations.[7-8,16,31] Moreover, it has been previously shown that the charge delocalization of the anion is not sufficient to avoid a strong interaction with the cation. For example, the thiocyanate anion (SCN-) also shows a strong interaction with cations of different sizes and charge density in various environments, even though it has a relatively delocalized charge and it is on the extreme of the Hofmeister series.[54-55,57,77]

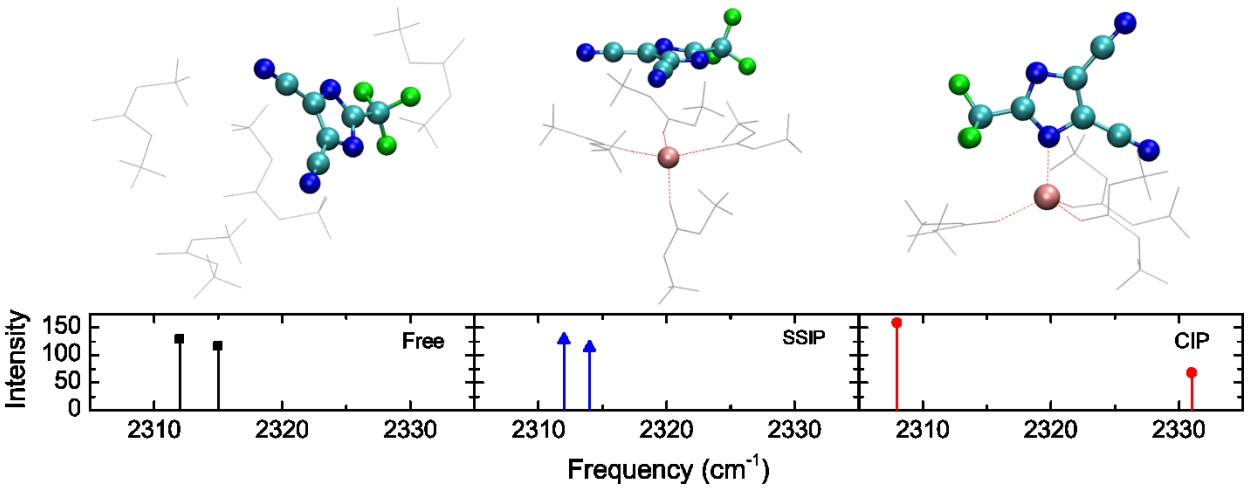

Figure 5. Structures and calculated vibrational frequencies for different species of anion association: free anion, solvent-separated ion pair (SSIP), and contact ion pair (CIP).

The proposed TDI speciation and IR CN stretch assignments are further tested by computing the vibrational modes of the possible different species using DFT computations. DFT frequency calculations of the CN stretches for free TDI-, solvent separated ion pair (SSIP), and CIP are presented in Figure 5. The free anion spectrum presents two nearly overlapping transitions located at 2312 cm^{-1} and 2315 cm^{-1} with similar intensities. Similarly, the SSIP spectrum shows two overlapping modes with similar intensities. In contrast, the CIP CN stretch modes are split into two distinct bands located at 2308 cm^{-1} and 2331 cm^{-1}, and the intensity of the low frequency mode is larger than that of the high frequency mode. The theoretical calculations show that the

growth of the high-frequency band in the CN region of the IR spectrum of TDI in either solvent only evidences the formation of CIPs. In addition, they demonstrate that the IR spectroscopy is not sensitive enough to differentiate between SSIPs and free ions as previously observed in other ions.[78-80]

The experimental data as well as the DFT frequency calculations provide a reasonable assignment of the FTIR bands of LiTDI in both solvents. However, the DFT frequency calculations also present some ambiguity. For example, DFT computations predict that the two CN stretches of the SSIP or free TDI- should appear at the same frequency as the low frequency band in the CIP. Thus, it is not possible to evaluate whether LiTDI in DMC is present as a mixture of CIPs and SSIPs or only CIPs. To this end, the spectrum of an equimolar mixture of LiTDI and (EMIM)TDI (X_{Li}=X_{EMIM}=0.05) in DMC was measured. In this case, the IR spectrum of the sample shows the same number of peaks and frequency positions as in the pure LiTDI, but the intensity of the high frequency peak decreases by half (see supporting information). The result indicates that LiTDI in DMC solution is composed in its majority by CIPs and that only LiTDI contributes to the formation of CIPs in DMC. In other words, the presence of extra TDI- in the solution does not change ion pair equilibrium (Li+ + TDI- ↔ LiTDI) because the anion is primarily as CIPs in the DMC solution. In addition, it is observed that the frequency position and width of the low frequency band of TDI- is not affected by the mixture, indicating that the difference in frequency between the EMIM+ and Li+ samples is likely to be caused by the difference in the dielectric constant of the solution due to the presence of the lithium salt.[81] These findings support the assertion that LiTDI does not form free ions or SSIPs in DMC, which is in agreement with the previous speciation of LiTDI in DMC.[38] However, our results indicate that TDI- is primarily found as free ion or SSIP in BC solutions. In addition, temperature-dependent FTIR performed on LiTDI

(X_{Li} = 0.05) in DMC and BC further supports our assignment, since it shows that the high frequency band at ~2245 cm^{-1} grows with increasing temperature irrespective of the solvent. This observation is in agreement with the CIP becoming more energetically favorable at high temperature due to a decrease of the Gibbs free energy of CIP formation with increasing temperature.[82] The temperature dependence of the Gibbs free energy in CIP formation is caused by the entropy term, which is positive because solvent molecules gain in the degrees of freedom when they are removed from the solvation shell of the ions as a consequence of ion pair formation.[82-83]

The structure and dynamics of TDI- in the organic carbonates were also derived from 2D IR spectroscopic experiments. The 2DIR spectra of LiTDI in DMC and BC (Figure 3) show two pairs of peaks with the lower frequency bands having higher intensity as seen in the linear IR (Figure 2). However, the second dimension allows one to observe a cross peak between the two diagonal peaks for both DMC and BC samples. The presence of a cross peak indicates a vibrational coupling between the two nitrile stretches modes of the anion.[45,75] In turn, the vibrational coupling confirms that some TDI- have a broken symmetry in their nearly degenerated CN stretches caused by the direct interaction of Li+ with TDI-. Thus, the presence of the cross peak further confirms the formation of CIPs and their vibrational signatures. While it is also possible that the cross peak arises from chemical exchange between SSIPs and free TDI and CIPs,[45] the presence of the cross peak at T_W=0 makes the exchange mechanism unlikely, since it implies a rate of ion pair formation comparable to the IR excitation pulse duration; i.e., ~50-60 fs.[46,58,84] Moreover, DFT computations predict a favorable energetics for the ion pair formation on the order of ~50 kcal/mol (see next section), which is significantly larger than the available thermal energy of system. In addition, the 2DIR spectra for (EMIM)TDI in either DMC or BC at various waiting times (Figure 3) display

only one set of peaks at 2225 cm^{-1}, but neither sample presents an obvious cross peak at T_W=0 ps. Thus, the cross peak seen in the 2DIR spectra corroborates the idea that CIPs species exist in both DMC and BC samples. Furthermore, the high frequency peak in the 2DIR spectra does not show evidence of an intraband cross peak at longer waiting times, which indicates that this peak does not contain two CIP transitions and only corresponds to the high frequency transition of the CIP as predicted by DFT calculations (Figure 5).

The dynamics of TDI- is derived from the 2DIR spectra using the center line slope (CLS) analysis.[85] The CLSs as a function of T_W for (EMIM)TDI and LiTDI in both pure DMC and pure BC are shown in Figure 6. The CLSs of the free anion from the (EMIM)TDI samples reveal an exponential decay dynamics of ~13 ps and ~12 ps (Table 1) for BC and DMC, respectively. The similarity between spectral diffusion characteristic times shows that both systems sense similar environments. In the case of the sample containing almost all of CIP, such as LiTDI in DMC, the peak at 2230 cm^{-1} shows a faster dynamics than the free ion and it has an offset (Table 1). While the difference in the dynamics evidences that the CN transitions might have a different mechanism for the frequency fluctuation, the offset in the CLS is related to the presence of multiple vibrational transitions associated to different configurations of the CIP, which are likely to exchange with much slower time constants than the investigated time window as previously seen for other CIPs.[46,86] Moreover, the residual of the CLS fitting of the 2230 cm^{-1} band shows the presence of an oscillation with a period of 9-30 cm^{-1}, which could arise from coherent vibrational energy transfer of the two CN mixed modes of TDI-,[87-88] since they are separated by ~20 cm^{-1} in DMC. Interestingly, the CLS of the high frequency peak, located at 2247 cm^{-1} and assigned to one transition of the CIP, exhibits a nearly constant behavior in both DMC and BC samples. The observed behavior might not be directly related to the solvation dynamics due to the excitonic

nature (strong coupling of the two CN stretches) of the vibrational modes. In other words, for two strong coupled and degenerated transitions, the vibrational Hamiltonian in the CN site representation can be written as:

$$\hat{H} = \begin{bmatrix} \omega_{10} + \delta\omega^1(t) & \beta(t) \\ \beta(t) & \omega_{10} + \delta\omega^2(t) \end{bmatrix}$$

where ω_{10} is the frequency of the two CN stretch modes of the molecule in the site representation, and $\beta(t)$ and $\delta\omega^i(t)$ are the coupling constant and the frequency fluctuation of the i^{th} site, respectively. For this vibrational Hamiltonian, the excitonic frequencies (eigenvalues) are given by:

$$\omega_{\pm} = \frac{2\omega_{10} + \delta\omega^1(t) + \delta\omega^2(t) \pm \sqrt{\left(\delta\omega^2(t) - \delta\omega^1(t)\right)^2 + 4\beta(t)^2}}{2}$$

where $\omega_{\pm}$ represents the frequencies of the symmetric and asymmetric stretch combinations. Thus, the frequencies in the exciton representation do not have a direct correspondence with individual site frequency fluctuations. The lack of CLS change is not surprising since a similar behavior has been previously reported for CIPs involving an anion with strong coupled transitions.[46,86] In contrast for the samples containing the TDI- mainly as free ions (i.e., LiTDI in BC), the low frequency transition of TDI- presents a slow, but observable, dynamics of the CLS (Figure 6 and Table 1). The slowdown of the CLS dynamics seen in BC might be associated to the formations of SSIPs, which limits the mobility of the solvent molecules in between TDI- and Li+ and results in a slower solvent dynamics than that experienced by the free anion. Finally, the contact ion pairing band at 2245 cm^{-1} of LiTDI in BC shows the nearly constant dynamics, which is in direct correspondence to the observed timescales for the CIP in the DMC solution.

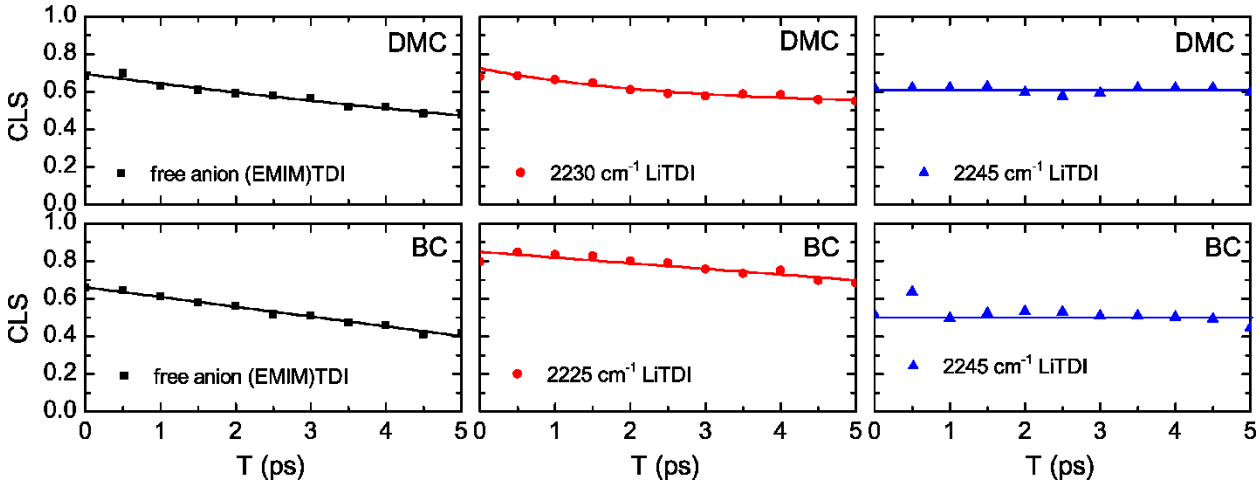

Figure 6. CLS analysis of the 2D IR bands of (EMIM)TDI (X_{EMIM} = 0.05) and LiTDI (X_{Li} = 0.05) in DMC and (EMIM)TDI (X_{EMIM} = 0.05) and LiTDI (X_{Li} = 0.05) in BC as a function of waiting time, T_W. Black squares correspond to (EMIM)TDI and red circles and blue triangles relate to the low and high frequency bands of LiTDI, respectively.

Salt	Solvent				
	DMC			BC	
	τ (ps)	A_0	y_0	τ (ps)	A_0
(EMIM)TDI	12.0*	0.69 ± 0.01	--	12.7*	0.662 ± 0.007
LiTDI (2230 cm^{-1})	2.5 ± 0.8**	0.19 ± 0.01	0.53 ± 0.03	23.7*	0.873 ± 0.008
LiTDI (2245 cm^{-1})	>100	0.728 ± 0.007	--	>100	0.58 ± 0.02

Table 1. Time constants and amplitudes for CLS fitting. *Time constants were derived from a linear fit (see supporting information). **Requires more than one exponential (see supporting information).

Solvent mixtures

In the previous section, it has been shown that the ability of LiTDI to form CIPs differs substantially by solvent structure (i.e., linear carbonate or cyclic carbonate). Thus, the effect of the solvent composition on the formation of CIPs is derived from the linear IR. The linear FTIR spectra of LiTDI (X_{Li} = 0.05) for various solvent mixtures shows that the CIP band at 2247 cm^{-1} monotonically rises with increasing DMC composition (Figure 4). This result is expected since LiTDI forms a larger amount of CIPs in DMC than BC, as seen in the linear IR of the pure solvents (Figure 2). However, it is apparent that the growth of the high frequency band is not linear. The nonlinear behavior is confirmed by plotting the ratio of peak intensities for the high and low bands

as a function of solvent composition (Figure 7). Remarkably, the amount of CIP appears to have two regions of linear regime. The first region comprises solvent composition from 0 to 0.6 molar fraction of DMC and has moderated change in the CIP concentration as a function of concentration of DMC. In contrast, the second region ranging from 0.8 to 1 of molar fraction of DMC shows a drastic change, where the amount of CIP is almost double while the solvent composition is only changed by less than 10%. The result clearly indicates that the composition of the Li+ solvation shell significantly affects the formation of CIPs in carbonate mixtures. It is also possible to infer that the lack of cyclic carbonates capable of solvating the cation directly affect the energetics of CIP formation. In other words, the CIP formation is promoted, or becomes energetically more favorable, when the Li+ solvation shell is primarily composed of the linear carbonate.

The hypothesis of Li+ having a more favorable CIP energetics for linear carbonates is corroborated by the ratio of the CN stretch bands of TDI- (X_{Li} = 0.05) in mixtures of pure linear carbonates and pure cyclic carbonates (Figure 4). The peak intensity ratios for the different mixtures (Figure 7) reveal the compelling difference between mixtures of pure linear or pure cyclic carbonates, where the CIP concentration remains nearly constant for different solvent ratios of the BC/PC and DMC/EMC mixtures, versus the mixtures of linear and cyclic carbonates, which exhibit rapid growth of CIP concentration with increasing DMC concentration in the DMC/BC mixtures. These results confirm that the trend is the result of two distinct carbonates (i.e., cyclic and linear) affecting differently the formation of CIPs.

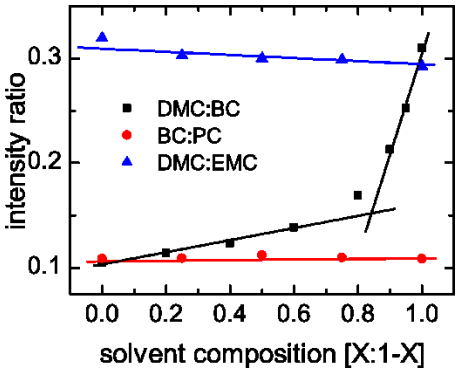

Figure 7. Plot of peak intensity ratio of high frequency band over low frequency band of the CN stretch of LiTDI as a function of the solvent composition for three different solvent mixtures: DMC:BC (black squares), BC:PC (red circles), and DMC:EMC (blue triangles). The plotted lines are guides to the eye.

The molecular mechanism behind the nonlinear trend seen in the CIP concentration as a function of the solvent composition is studied by DFT computations. One potential cause for explaining the difference in the CIP formation is the capacity of the solvent molecules to delocalize the charge of Li+. In other words, it is expected that the solvation shell that better delocalizes the positive charge of Li+ should be less susceptible to form CIPs. To test this possibility, the charge of Li+ in the five possible tetrahedral solvation shells was determined using natural bond orbital analysis (see methods section). The results (Table 2) show that there is very little change in the charge of Li+ as a function of the composition of the solvation shell. Thus, it is unlikely that the observed trend is merely due to a charge delocalization.

	Solvation shell structure $Li(BC)_{4-X}(DMC)_X$				
	0	1	2	3	4
Li+ charge	0.67	0.67	0.67	0.67	0.69

Table 2. Li+ charge as a function of solvation shell composition computed by ab-initio simulations.

Another possible explanation for the nonlinear growth of the CIP concentration in the solvent mixture is related to the energetics of CIP formation (i.e., Li+ + TDI- ↔ LiTDI). It has been previously inferred that the solvation shell composition plays a significant role in the

energetics of CIP formation.[5,17,24,89] Thus, to test this possibility the energy trends for the formation of CIP as a function of the solvation shell composition were computed using DFT calculations. The results of these energy calculations are summarized in Figure 8. In addition, a table containing all possible solvation shells investigated can be found in the supporting information. The energetics shows that the internal energy (ΔE) of CIP formation is highly influenced by the composition of the solvation shell, where larger amount of the linear carbonates in the Li+ solvation shell makes more favorable the CIP formation. This theoretical result is in line with the experimental observations. Moreover, the computations predict an energy difference of ~35 kJ/mol in the stabilization of the CIP when switching from a pure BC to a pure DMC solvation shell, which explains the difference in CIP concentration observed for LiTDI in the two pure carbonates. Additionally, the computational results (Figure 8) shows that decreasing BC participation in the Li+ solvation shell results in a non-linear decrease of ΔE of CIP formation.

The equilibrium constant K for CIP formation can be computed from the Gibbs free energy as:

$$K = exp(-\Delta G/RT) = exp\left(-\frac{\Delta H}{RT} + \frac{\Delta S}{R}\right)$$

where ΔH and ΔS are the change in enthalpy and entropy of the reaction. Assuming that ΔH≈ΔE and that the ΔS is the same for all the CIP formation reactions, the ratio of the two equilibrium constants associated with two different solvation shells is given by:

$$K_i/K_j = exp\left(-\frac{\Delta E_i - \Delta E_j}{RT}\right)$$

where *i* and *j* represent different conditions of the system. The value of the K_i/K_0, computed for the different energetic values corresponding to different solvent compositions and taking as

reference the equilibrium constant of CIP formation (K_0) for pure BC, is presented in Figure 8. The K_i/K_0 for the different equilibrium constants shows an exponential increase with increasing DMC participation in the solvation shell, which mirrors the trend of the experimental data (Figure 7). These results confirm that number and structure of the carbonate in the Li+ solvation defines the energetics of CIP formation in LiTDI. Specifically, Li+ solvation shells with a greater concentration of DMC have the most energetically favorable CIP formation, while higher BC content in the Li+ solvation shell convenes a stabilization to the solvation shell against the CIP formation.

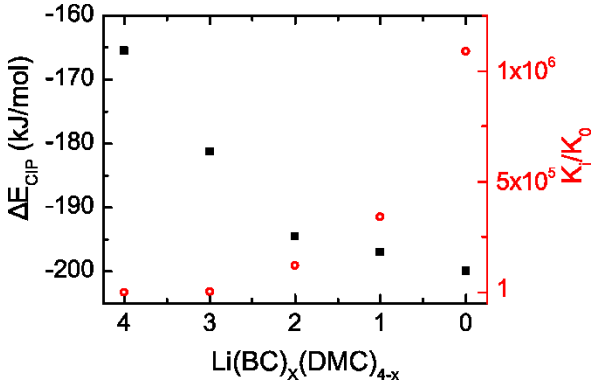

Figure 8. Energy and equilibrium constant of CIP formation as a function of solvation shell composition of the free ion. The change in internal energy is shown as black squares and the equilibrium constant is shown in red circles.

The result predicted via DFT computations is confirmed by FTIR spectroscopic experiments. In this case, the amount of CIP is derived from a sample containing LiTDI and LiTFSI in DMC (X_{Li} = 0.07 and X_{TDI}=0.05), where the excess of Li+ is expected to drive TDI- to form quantitative amounts of CIP. From the areas derived from fitting the spectra of X_{Li} = 0.05 LiTDI in DMC, X_{Li} = 0.05 LiTDI in BC, and X_{Li} = 0.07 LiTDI/LiTFSI in DMC (see supporting information), the corresponding equilibrium constants of CIP formation were calculated. The computed equilibrium constants from the experimental results are summarized in Table 3. Approximately 6% of the species in X_{Li} = 0.05 LiTDI in DMC are free ions, while the BC sample

is dominated by free anions (74%). Thus, the experimental equilibrium constants show a change in two to three orders of magnitude. This result is in line with the DFT computations where a significant preference for CIP formation is observed for DMC over BC as seen by the computed equilibrium constant ratio. Note that the difference between the equilibrium constants computed from DFT and the experiments could arise from neglecting the entropic part of the Gibbs free energy, which might not be a good approximation in the case of linear carbonates since they can undergo conformational changes.

X_{Li} = 0.05 LiTDI	Percent of free anion	K_{eq}
in DMC	6%	310
in BC	74%	0.5

Table 3. Experimental fraction of free anion and equilibrium constants (K_{eq}) derived from ratio of FTIR areas.

SUMMARY

Our study shows that at relatively low concentration LiTDI solution, X_{Li}=0.05 which is approximately half the concentration of Li+ used in commercial batteries, the speciation of Li+ is highly dependent on the solvent molecular structure. In particular, when the solvent is a linear carbonate, the Li+ and TDI- exist predominantly as a CIP. In contrast for cyclic carbonates, Li+ and TDI- are primarily found as free ion and SSIP species. Interestingly, the speciation of Li+ is also highly dependent on the presence of cyclic components in mixtures of linear and cyclic carbonates. Specifically, there is a drastic increase of the CIP concentration with increasing concentration of the linear carbonate. The molecular origin of this behavior is obtained by DFT computations, which reveal that the energetics of ion pair formation is less favored when Li+ contains cyclic carbonates in its solvation shell. Overall, this study provides a molecular-level picture of ion pair formation and its relation to the solvent structure and composition. Thus, the

presented results are relevant to the energy storage industry, where mixtures of linear and cyclic organic carbonates are commonly used for making commercial lithium ion batteries.

ASSOCIATED CONTENT

Supporting Information

The Supporting Information is available free of charge on the ACS Publications website at DOI:

FTIR spectrum of a mixture of (EMIM)TDI and LiTDI and a mixture of LiTFSI and LiTDI (Figure S1); 2DIR spectra for 2DIR spectra for waiting times of 10 and 15 ps (Figure S2); difference FTIR spectra for the CN stretch region as function of temperature (Figure S3); Slice of the 2DIR spectra of LiTDI in BC as function of waiting time (Figure S4); fitting with exponential decays of the CLS of the 2230 cm-1 band for TDI- in DMC (Figure S5); fitting of the residuals of the CLS fitting of the 2230 cm-1 band for TDI- in DMC (Figure S6); derivation of tau from linear fit; calculation of contact ion pair equilibrium constants; oscillator strength of the CN stretch of TDI- as function of speciation; internal energy of contact ion pair formation for all calculated solvation shells (Table S1 and Figure S7) and.

AUTHOR INFORMATION

Corresponding Author

* E-mail: dkuroda@lsu.edu. Tel: (+1) 225-578-1780

ORCID

Daniel G. Kuroda: 0000-0002-4752-7024

NOTES

The authors declare no competing financial interest.

ACKNOWLEDGMENTS

The authors acknowledge financial support from the National Science Foundation (CHE-1751735). The authors also acknowledge the High Performance Computing Center at Louisiana State University and the Louisiana Optical Network Initiative (LONI) for computer time.

REFERENCES

1. Aifantis, K. E.; Hackney, S. A.; Kumar, R. V., *High energy density lithium batteries : Materials, engineering, applications*. Wiley-VCH: Weinheim, 2010.
2. Armand, M.; Tarascon, J. M., Building better batteries. *Nature* **2008,** *451* (7179), 652-657.
3. Divya, K. C.; Ostergaard, J., Battery energy storage technology for power systems-an overview. *Electr. Pow. Syst. Res.* **2009,** *79* (4), 511-520.
4. Dunn, B.; Kamath, H.; Tarascon, J. M., Electrical energy storage for the grid: A battery of choices. *Science* **2011,** *334* (6058), 928-935.
5. Xu, K., Electrolytes and interphases in li-ion batteries and beyond. *Chem. Rev.* **2014,** *114* (23), 11503-11618.
6. Xu, K., Nonaqueous liquid electrolytes for lithium-based rechargeable batteries. *Chem. Rev.* **2004,** *104* (10), 4303-4417.
7. Fulfer, K. D.; Kuroda, D. G., Solvation structure and dynamics of the lithium ion in organic carbonate-based electrolytes: A time-dependent infrared spectroscopy study. *J. Phys. Chem. C* **2016,** *120* (42), 24011-24022.
8. Seo, D. M.; Reininger, S.; Kutcher, M.; Redmond, K.; Euler, W. B.; Lucht, B. L., Role of mixed solvation and ion pairing in the solution structure of lithium ion battery electrolytes. *J. Phys. Chem. C* **2015,** *119* (25), 14038-14046.
9. Zhang, X. L.; Kuroda, D. G., An ab initio molecular dynamics study of the solvation structure and ultrafast dynamics of lithium salts in organic carbonates: A comparison between linear and cyclic carbonates. *J. Chem. Phys.* **2019,** *150* (18), 184501.
10. Aroca, R.; Nazri, R.; Nazri, G. A.; Camargo, A. J.; Trsic, M., Vibrational spectra and ion-pair properties of lithium hexafluorophosphate in ethylene carbonate based mixed-solvent systems for lithium batteries. *J. Solution Chem.* **2000,** *29* (10), 1047-1060.
11. Giorgini, M. G.; Futamatagawa, K.; Torii, H.; Musso, M.; Cerini, S., Salvation structure around the li+ ion in mixed cyclic/linear carbonate solutions unveiled by the raman noncoincidence effect. *J. Phys. Chem. Lett.* **2015,** *6* (16), 3296-3302.
12. Cresce, A. V.; Borodin, O.; Xu, K., Correlating li+ solvation sheath structure with interphasial chemistry on graphite. *J. Phys. Chem. C* **2012,** *116* (50), 26111-26117.
13. Ding, M. S., Electrolytic conductivity and glass transition temperature as functions of salt content, solvent composition, or temperature for lipf6 in propylene carbonate plus diethyl carbonate. *J. Chem. Eng. Data* **2003,** *48* (3), 519-528.

14. Ding, M. S.; Xu, K.; Zhang, S. S.; Amine, K.; Henriksen, G. L.; Jow, T. R., Change of conductivity with salt content, solvent composition, and temperature for electrolytes of lipf6 in ethylene carbonate-ethyl methyl carbonate. *J. Electrochem. Soc.* **2001,** *148* (10), A1196-A1204.
15. Wang, J. H.; Yamada, Y.; Sodeyama, K.; Chiang, C. H.; Tateyama, Y.; Yamada, A., Superconcentrated electrolytes for a high-voltage lithium-ion battery. *Nat. Commun.* **2016,** *7*, 12032.
16. Chapman, N.; Borodin, O.; Yoon, T.; Nguyen, C. C.; Lucht, B. L., Spectroscopic and density functional theory characterization of common lithium salt solvates in carbonate electrolytes for lithium batteries. *J. Phys. Chem. C* **2017,** *121* (4), 2135-2148.
17. Fulfer, K. D.; Kuroda, D. G., Ion speciation of lithium hexafluorophosphate in dimethyl carbonate solutions: An infrared spectroscopy study. *PCCP* **2018,** *20* (35), 22710-22718.
18. Xu, K.; Cresce, A. V., Li+-solvation/desolvation dictates interphasial processes on graphitic anode in li ion cells. *J. Mater. Res.* **2012,** *27* (18), 2327-2341.
19. Xu, K.; Von Cresce, A., Li+-solvation structure directs interphasial processes on graphitic anodes. *ECS Trans.* **2012,** *41* (41), 187-193.
20. Morita, M.; Asai, Y.; Yoshimoto, N.; Ishikawa, M., A raman spectroscopic study of organic electrolyte solutions based on binary solvent systems of ethylene carbonate with low viscosity solvents which dissolve different lithium salts. *J. Chem. Soc., Faraday Trans.* **1998,** *94* (23), 3451-3456.
21. Hyodo, S. A.; Okabayashi, K., Raman intensity study of local-structure in non-aqueous electrolyte-solutions .2. Cation solvent interaction in mixed-solvent systems and selective solvation. *Electrochim. Acta* **1989,** *34* (11), 1557-1561.
22. Delp, S. A.; Borodin, O.; Olguin, M.; Eisner, C. G.; Allen, J. L.; Jow, T. R., Importance of reduction and oxidation stability of high voltage electrolytes and additives. *Electrochim. Acta* **2016,** *209*, 498-510.
23. Brodin, A.; Jacobsson, P., Dipolar interaction and molecular ordering in liquid propylene carbonate: Anomalous dielectric susceptibility and raman non-coincidence effect. *J. Mol. Liq.* **2011,** *164* (1), 17-21.
24. Borodin, O.; Olguin, M.; Ganesh, P.; Kent, P. R. C.; Allen, J. L.; Henderson, W. A., Competitive lithium solvation of linear and cyclic carbonates from quantum chemistry. *PCCP* **2016,** *18* (1), 164-175.
25. Bogle, X.; Vazquez, R.; Greenbaum, S.; Cresce, A. V.; Xu, K., Understanding li+-solvent interaction in nonaqueous carbonate electrolytes with o-17 nmr. *J. Phys. Chem. Lett.* **2013,** *4* (10), 1664-1668.
26. Skarmoutsos, I.; Ponnuchamy, V.; Vetere, V.; Mossa, S., Li+ solvation in pure, binary, and ternary mixtures of organic carbonate electrolytes. *J. Phys. Chem. C* **2015,** *119* (9), 4502-4515.
27. von Cresce, A.; Xu, K., Preferential solvation of li+ directs formation of interphase on graphitic anode. *Electrochem. Solid-State Lett.* **2011,** *14* (10), A154-A156.
28. Wang, J. J.; Wu, Y. P.; Xuan, X. P.; Wang, H. Q., Ion-molecule interactions in solutions of lithium perchlorate in propylene carbonate plus diethyl carbonate mixtures: An ir and molecular orbital study. *Spectrochim. Acta, Part A* **2002,** *58* (10), 2097-2104.
29. Ue, M.; Mori, S., Mobility and ionic association of lithium-salts in a propylene carbonate-ethyl methyl carbonate mixed-solvent. *J. Electrochem. Soc.* **1995,** *142* (8), 2577-2581.
30. Xu, K.; Lam, Y. F.; Zhang, S. S.; Jow, T. R.; Curtis, T. B., Solvation sheath of li+ in nonaqueous electrolytes and its implication of graphite/electrolyte interface chemistry. *J. Phys. Chem. C* **2007,** *111* (20), 7411-7421.

31. Maeda, S.; Kameda, Y.; Amo, Y.; Usuki, T.; Ikeda, K.; Otomo, T.; Yanagisawa, M.; Seki, S.; Arai, N.; Watanabe, H., et al., Local structure of li+ in concentrated ethylene carbonate solutions studied by low-frequency raman scattering and neutron diffraction with li-6/li-7 isotopic substitution methods. *J. Phys. Chem. B* **2017,** *121* (48), 10979-10987.
32. Fulfer, K. D.; Kuroda, D. G., A comparison of the solvation structure and dynamics of the lithium ion in linear organic carbonates with different alkyl chain lengths. *PCCP* **2017,** *19* (36), 25140-25150.
33. Dranka, M.; Niedzicki, L.; Kasprzyk, M.; Marcinek, M.; Wieczorek, W.; Zachara, J., An insight into coordination ability of dicyanoimidazolato anions toward lithium in presence of acetonitrile. Crystal structures of novel lithium battery electrolyte salts. *Polyhedron* **2013,** *51*, 111-116.
34. Scheers, J.; Niedzicki, L.; Zukowska, G. Z.; Johansson, P.; Wieczorek, W.; Jacobsson, P., Ion-ion and ion-solvent interactions in lithium imidazolide electrolytes studied by raman spectroscopy and dft models. *PCCP* **2011,** *13* (23), 11136-11147.
35. Niedzicki, L.; Kasprzyk, M.; Kuziak, K.; Zukowska, G. Z.; Marcinek, M.; Wieczorek, W.; Armand, M., Liquid electrolytes based on new lithium conductive imidazole salts. *J. Power Sources* **2011,** *196* (3), 1386-1391.
36. Niedzicki, L.; Kasprzyk, M.; Kuziak, K.; Zukowska, G. Z.; Armand, M.; Bukowska, M.; Marcinek, M.; Szczecinski, P.; Wieczorek, W., Modern generation of polymer electrolytes based on lithium conductive imidazole salts. *J. Power Sources* **2009,** *192* (2), 612-617.
37. Jankowski, P.; Zukowska, G. Z.; Dranka, M.; Marczewski, M. J.; Ostrowski, A.; Korczak, J.; Niedzicki, L.; Zalewska, A.; Wieczorek, W., Understanding of lithium 4,5-dicyanoimidazolate-poly(ethylene oxide) system: Influence of the architecture of the solid phase on the conductivity. *J. Phys. Chem. C* **2016,** *120* (41), 23358-23367.
38. Niedzicki, L.; Karpierz, E.; Bitner, A.; Kasprzyk, M.; Zukowska, G. Z.; Marcinek, M.; Wieczorek, W., Optimization of the lithium-ion cell electrolyte composition through the use of the litdi salt. *Electrochim. Acta* **2014,** *117*, 224-229.
39. Niedzicki, L.; Karpierz, E.; Zawadzki, M.; Dranka, M.; Kasprzyk, M.; Zalewska, A.; Marcinek, M.; Zachara, J.; Domanska, U.; Wieczorek, W., Lithium cation conducting tdi anion-based ionic liquids. *PCCP* **2014,** *16* (23), 11417-11425.
40. Scheers, J.; Johansson, P.; Szczecinski, P.; Wieczorek, W.; Armand, M.; Jacobsson, P., Benzimidazole and imidazole lithium salts for battery electrolytes. *J. Power Sources* **2010,** *195* (18), 6081-6087.
41. McOwen, D. W.; Delp, S. A.; Paillard, E.; Herriot, C.; Han, S. D.; Boyle, P. D.; Sommer, R. D.; Henderson, W. A., Anion coordination interactions in solvates with the lithium salts lidcta and litdi. *J. Phys. Chem. C* **2014,** *118* (15), 7781-7787.
42. Barthel, J.; Buchner, R.; Wismeth, E., Ftir spectroscopy of ion solvation of liclo4 and liscn in acetonitrile, benzonitrile, and propylene carbonate. *J. Solution Chem.* **2000,** *29* (10), 937-954.
43. Niedzicki, L.; Grugeon, S.; Laruelle, S.; Judeinstein, P.; Bukowska, M.; Prejzner, J.; Szczecinski, P.; Wieczorek, W.; Armand, M., New covalent salts of the 4+v class for li batteries. *J. Power Sources* **2011,** *196* (20), 8696-8700.
44. Berhaut, C. L.; Porion, P.; Timperman, L.; Schmidt, G.; Lemordant, D.; Anouti, M., Litdi as electrolyte salt for li-ion batteries: Transport properties in ec/dmc. *Electrochim. Acta* **2015,** *180*, 778-787.
45. Hamm, P.; Zanni, M. T., *Concepts and methods of 2d infrared spectroscopy*. Cambridge University Pres: Cambridge ; New York, 2011; p ix, 286 p.

46. Kuroda, D. G.; Hochstrasser, R. M., Two-dimensional infrared spectral signature and hydration of the oxalate dianion. *J. Chem. Phys.* **2011,** *135* (20), 204502.
47. Cui, Y. W.; Kuroda, D. G., Evidence of molecular heterogeneities in amide-based deep eutectic solvents. *J. Phys. Chem. A* **2018,** *122* (5), 1185-1193.
48. Kim, Y. S.; Wang, J. P.; Hochstrasser, R. M., Two-dimensional infrared spectroscopy of the alanine dipeptide in aqueous solution. *J. Phys. Chem. B* **2005,** *109* (15), 7511-7521.
49. Vorobyev, D. Y.; Kuo, C. H.; Kuroda, D. G.; Scott, J. N.; Vanderkooi, J. M.; Hochstrasser, R. M., Water-induced relaxation of a degenerate vibration of guanidium using 2d ir echo spectroscopy. *J. Phys. Chem. B* **2010,** *114* (8), 2944-2953.
50. Hunt, N. T., 2d-ir spectroscopy: Ultrafast insights into biomolecule structure and function. *Chem. Soc. Rev.* **2009,** *38* (7), 1837-1848.
51. Fayer, M. D., Dynamics of liquids, molecules, and proteins measured with ultrafast 2d ir vibrational echo chemical exchange spectroscopy. *Annu. Rev. Phys. Chem.* **2009,** *60*, 21-38.
52. Sun, Z.; Zhang, W. K.; Ji, M. B.; Hartsock, R.; Gaffney, K. J., Contact ion pair formation between hard acids and soft bases in aqueous solutions observed with 2dir spectroscopy. *J. Phys. Chem. B* **2013,** *117* (49), 15306-15312.
53. Park, K. H.; Choi, S. R.; Choi, J. H.; Park, S.; Cho, M., Real-time probing of ion pairing dynamics with 2dir spectroscopy. *ChemPhysChem* **2010,** *11* (17), 3632-3637.
54. Ji, M. B.; Park, S.; Gaffney, K. J., Dynamics of ion assembly in solution: 2dir spectroscopy study of lincs in benzonitrile. *J. Phys. Chem. Lett.* **2010,** *1* (12), 1771-1775.
55. Bian, H. T.; Chen, H. L.; Zhang, Q.; Li, J. B.; Wen, X. W.; Zhuang, W.; Zheng, J. R., Cation effects on rotational dynamics of anions and water molecules in alkali (li+, na+, k+, cs+) thiocyanate (scn-) aqueous solutions. *J. Phys. Chem. B* **2013,** *117* (26), 7972-7984.
56. Yuan, R. F.; Yan, C.; Fayer, M., Ion-molecule complex dissociation and formation dynamics in licl aqueous solutions from 2d ir spectroscopy. *J. Phys. Chem. B* **2018,** *122* (46), 10582-10592.
57. Roy, V. P.; Kubarych, K. J., Interfacial hydration dynamics in cationic micelles using 2d-ir and nmr. *J. Phys. Chem. B* **2017,** *121* (41), 9621-9630.
58. Kuroda, D. G.; Abdo, M.; Chuntonov, L.; Smith, A. B.; Hochstrasser, R. M., Vibrational dynamics of a non-degenerate ultrafast rotor: The (c12,c13)-oxalate ion. *J. Chem. Phys.* **2013,** *139* (16), 164514.
59. Johansson, P.; Beranger, S.; Armand, M.; Nilsson, H.; Jacobsson, P., Spectroscopic and theoretical study of the 1,2,3-triazole-4,5-dicarbonitrile anion and its lithium ion pairs. *Solid State Ionics* **2003,** *156* (1-2), 129-139.
60. Stoyanov, S. S., Scaling of computed cyano-stretching frequencies and ir intensities of nitriles, their anions, and radicals. *J. Phys. Chem. A* **2010,** *114* (15), 5149-5161.
61. Xuan, X. P.; Zhang, H. C.; Wang, J. J.; Wang, H. Q., Vibrational spectroscopic and density functional studies on ion solvation and association of lithium tetrafluorobrate in acetonitrile. *J. Phys. Chem. A* **2004,** *108* (37), 7513-7521.
62. Coetzee, J. F.; Sharpe, W. R., Solute-solvent interactions. Vii. Proton magnetic resonance and infrared study of ion solvation in dipolar aprotic solvents. *J. Solution Chem.* **1972,** *1* (1), 77-91.
63. Niedzicki, L.; Zukowska, G. Z.; Bukowska, M.; Szczecinski, P.; Grugeon, S.; Laruelle, S.; Armand, M.; Panero, S.; Scrosati, B.; Marcinek, M., et al., New type of imidazole based salts designed specifically for lithium ion batteries. *Electrochim. Acta* **2010,** *55* (4), 1450-1454.

64. Asplund, M. C.; Zanni, M. T.; Hochstrasser, R. M., Two-dimensional infrared spectroscopy of peptides by phase-controlled femtosecond vibrational photon echoes. *Proc. Natl. Acad. Sci. U.S.A.* **2000,** *97* (15), 8219-8224.
65. Eckbreth, A. C., Boxcars - crossed-beam phase-matched cars generation in gases. *Appl. Phys. Lett.* **1978,** *32* (7), 421-423.
66. Frisch, M. J.; Trucks, G. W.; Schlegel, H. B.; Scuseria, G. E.; Robb, M. A.; Cheeseman, J. R.; Scalmani, G.; Barone, V.; Petersson, G. A.; Nakatsuji, H., et al. *Gaussian 09*, Wallingford, CT, 2016.
67. Bauschlicher, C. W.; Haskins, J. B.; Bucholz, E. W.; Lawson, J. W.; Borodin, O., Structure and energetics of li+-(bf4-)(n ') li+-(fsi-)(n '), and li+-(tfsi-)(n): Ab initio and polarizable force field approaches. *J. Phys. Chem. B* **2014,** *118* (36), 10785-10794.
68. Korsun, O. M.; Kalugin, O. N.; Fritsky, I. O.; Prezhdo, O. V., Ion association in aprotic solvents for lithium ion batteries requires discrete-continuum approach: Lithium bis(oxalato)borate in ethylene carbonate based mixtures. *J Phys Chem C* **2016,** *120* (30), 16545-16552.
69. Jiang, B.; Ponnuchamy, V.; Shen, Y.; Yang, X.; Yuan, K.; Vetere, V.; Mossa, S.; Skarmoutsos, I.; Zhang, Y.; Zheng, J., The anion effect on li+ ion coordination structure in ethylene carbonate solutions. *J. Phys. Chem. Lett.* **2016,** *7* (18), 3554-3559.
70. Ponnuchamy, V.; Mossa, S.; Skarmoutsos, I., Solvent and salt effect on lithium ion solvation and contact ion pair formation in organic carbonates: A quantum chemical perspective. *J. Phys. Chem. C* **2018,** *122* (45), 25930-25939.
71. Foster, J. P.; Weinhold, F., Natural hybrid orbitals. *J. Am. Chem. Soc.* **1980,** *102* (24), 7211-7218.
72. Rives, A. B.; Weinhold, F., Natural hybrid orbitals - abinitio scf and ci results for co and nico. *Int. J. Quantum Chem.* **1980,** *17*, 201-209.
73. Reed, A. E.; Weinhold, F., Natural bond orbital analysis of near-hartree-fock water dimer. *J. Chem. Phys.* **1983,** *78* (6), 4066-4073.
74. Ghosh, A.; Remorino, A.; Tucker, M. J.; Hochstrasser, R. M., 2d ir photon echo spectroscopy reveals hydrogen bond dynamics of aromatic nitriles. *Chem. Phys. Lett.* **2009,** *469* (4-6), 325-330.
75. Golonzka, O.; Khalil, M.; Demirdoven, N.; Tokmakoff, A., Coupling and orientation between anharmonic vibrations characterized with two-dimensional infrared vibrational echo spectroscopy. *J. Chem. Phys.* **2001,** *115* (23), 10814-10828.
76. Ohta, K.; Tominaga, K., Vibrational population relaxation of thiocyanate ion in polar solvents studied by ultrafast infrared spectroscopy. *Chem. Phys. Lett.* **2006,** *429* (1-3), 136-140.
77. Lee, K. K.; Park, K. H.; Kwon, D.; Choi, J. H.; Son, H.; Park, S.; Cho, M., Ion-pairing dynamics of li+ and scn- in dimethylformamide solution: Chemical exchange two-dimensional infrared spectroscopy. *J. Chem. Phys.* **2011,** *134* (6), 064506.
78. Zhang, X.; Kumar, R.; Kuroda, D. G., Acetate ion and its interesting solvation shell structure and dynamics. *J. Chem. Phys.* **2018,** *148* (9), 094506.
79. Kankanamge, S. R. G.; Kuroda, D. G., Molecular structure and ultrafast dynamics of sodium thiocyanate ion pairs formed in glymes of different lengths. *PCCP* **2019,** *21* (2), 833-841.
80. Hefter, G., When spectroscopy fails: The measurement of ion pairing. *Pure Appl. Chem.* **2006,** *78* (8), 1571-1586.
81. Wang, P. M.; Anderko, A., Computation of dielectric constants of solvent mixtures and electrolyte solutions. *Fluid Phase Equilib.* **2001,** *186* (1-2), 103-122.

82. Marcus, Y.; Hefter, G., Ion pairing. *Chem. Rev.* **2006,** *106* (11), 4585-4621.
83. Prue, J. E., Ion pairs and complexes - free energies enthalpies and entropies. *J. Chem. Educ.* **1969,** *46* (1), 12.
84. Kim, Y. S.; Hochstrasser, R. M., Chemical exchange 2d ir of hydrogen-bond making and breaking. *Proc. Natl. Acad. Sci. U.S.A.* **2005,** *102* (32), 11185-11190.
85. Kwak, K.; Park, S.; Finkelstein, I. J.; Fayer, M. D., Frequency-frequency correlation functions and apodization in two-dimensional infrared vibrational echo spectroscopy: A new approach. *J. Chem. Phys.* **2007,** *127* (12), 124503.
86. Kuroda, D. G.; Hochstrasser, R. M., Dynamic structures of aqueous oxalate and the effects of counterions seen by 2d ir. *PCCP* **2012,** *14* (18), 6219-6224.
87. He, X. M.; Yu, P. Y.; Zhao, J.; Wang, J. P., Efficient vibrational energy transfer through covalent bond in indigo carmine revealed by nonlinear ir spectroscopy. *J. Phys. Chem. B* **2017,** *121* (40), 9411-9421.
88. Wong, D. B.; Giammanco, C. H.; Fenn, E. E.; Fayer, M. D., Dynamics of isolated water molecules in a sea of ions in a room temperature ionic liquid. *J. Phys. Chem. B* **2013,** *117* (2), 623-635.
89. Borodin, O.; Smith, G. D., Quantum chemistry and molecular dynamics simulation study of dimethyl carbonate: Ethylene carbonate electrolytes doped with lipf6. *J. Phys. Chem. B* **2009,** *113* (6), 1763-1776.